Supporting Information

Highly reversible and fast sodium storage boosted by improved interfacial and surface charge transfer derived from the synergistic effect of heterostructures and pseudocapacitance in SnO_2-based anodes

Xin Li[a], Xiaohong Sun[a,*], Zhiwen Gao[a], Xudong Hu[a], Rui Ling[a], Shu Cai[a], Chunming Zheng[b,*], Wenbin Hu[a]

[a]*School of Materials Science and Engineering, Key Laboratory of Advanced Ceramics and Machining Technology of Ministry of Education, Tianjin University, Tianjin 300072, PR China*

[b]*State Key Laboratory of Hollow-fiber Membrane Materials and Membrane Processes, School of Environmental and Chemical Engineering, Tianjin Polytechnic University, Tianjin 300387, PR China*

* Corresponding authors.

*Tel.:+86-22-85356661. Fax: +86-22-85356661. E-mail: sunxh@tju.edu.cn.

*Tel.:+86-22-83955661. Fax: +86-22-83955661. E-mail: zhengchunming@tjpu.edu.cn.

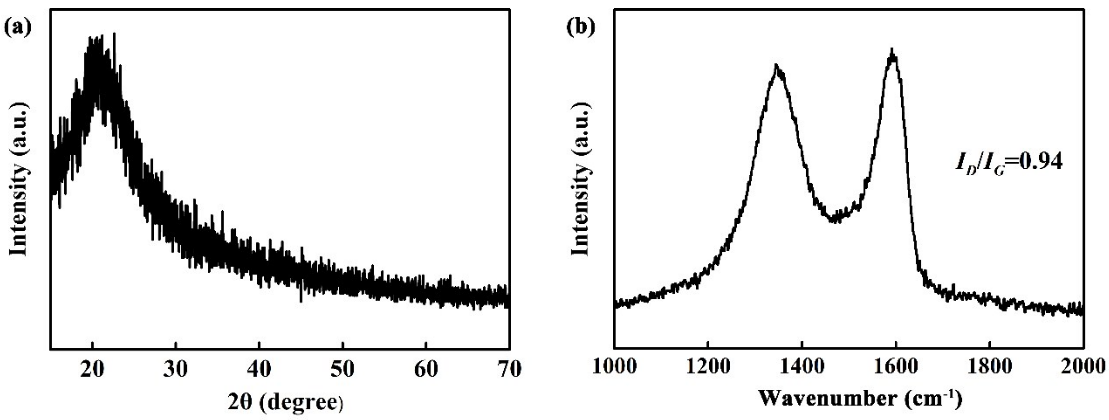

Fig. S1 (a) XRD pattern and (b) Raman spectrum of graphene oxide.

Synthesis of graphene oxide/Co_3O_4: The preparation of graphene oxide/Co_3O_4 was briefly stated as followed. Graphene oxide (GO) (0.04 g) was put into 40 mL deionized water followed by ultrasonic process for 1 h. Then 0.27 g $Co(NO_3)_2 \cdot 6H_2O$ and 15 mL ammonia solution (28 wt%) was mixed with GO suspension by ultrasonic for 1 h. Afterwards the mixture suspension was transferred into a Teflon-lined stainless-steel autoclave, sealed and hydrothermally treated at 180 ºC for 24 h. The obtained precipitate was washed with deionized water and ethanol and dried at 80 ºC for 10 h.

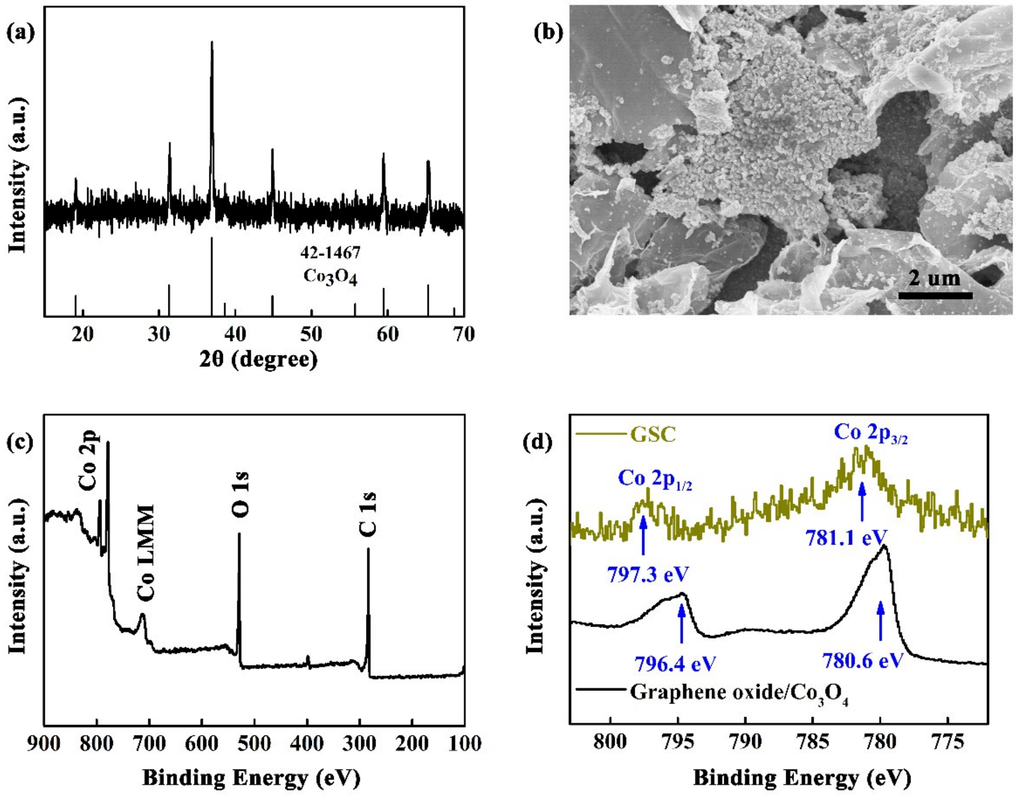

Fig. S2 (a) XRD pattern, (b) SEM image, and (c) XPS survey spectra of graphene oxide/Co_3O_4. (d) The corresponding Co 2p XPS spectrum of GSC and graphene oxide/Co_3O_4. The peaks of 797.3 eV and 781.1 eV are ascribed to Co $2p_{1/2}$ and Co $2p_{3/2}$ in GSC and the peaks of 796.4 eV and 780.6 eV are ascribed to Co $2p_{1/2}$ and Co $2p_{3/2}$ in graphene oxide/Co_3O_4. It is obviously that the two peaks of Co 2p for GSC both shifted to higher binding energies compared to those for graphene oxide/Co_3O_4, revealing that the 2p electron in Co is interacting with the adjacent SnO_2 for GSC sample.

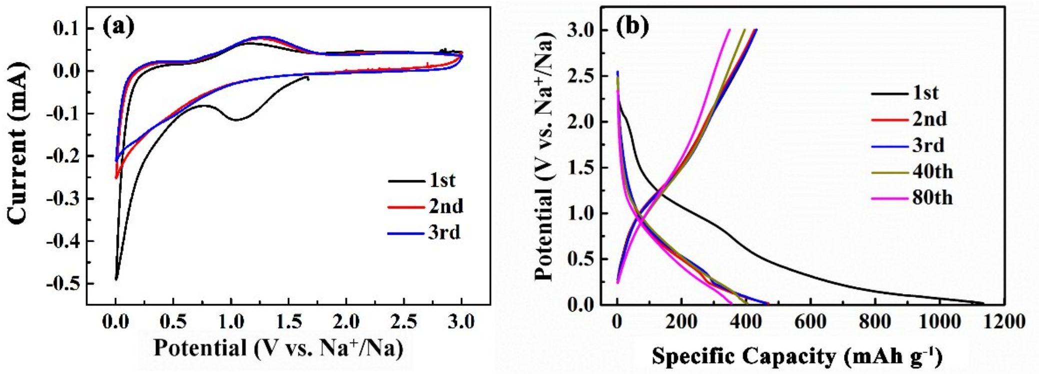

Fig. S3 (a) Cyclic voltammetry (CV) profiles of GS at a scan rate of 0.1 mV s^{-1}. (b) Galvanostatic discharge-charge profiles of GS within the potential window of 0.01-3.0 V at a current density of 0.1 A g^{-1}.

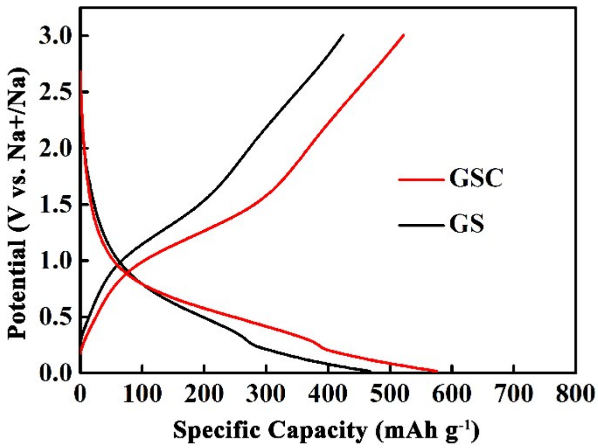

Fig. S4 Galvanostatic discharge-charge profiles of GSC and GS of the second cycle within the potential window of 0.01-3.0 V at a current density of 0.1 A g^{-1}.

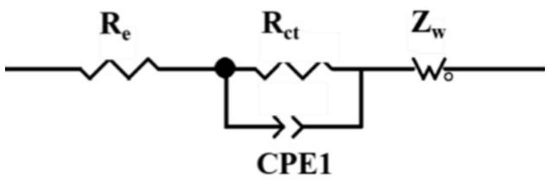

Fig. S5 The equivalent circuit used for the analysis of the impedance plots. R_e is the electrolyte resistance and the resistance of the surface film formed on the electrodes. R_{ct} is charge-transfer resistance, Z_w is the Warburg impedance related to the diffusion of sodium ions into the bulk electrodes and CPE1 represents the constant phase element.

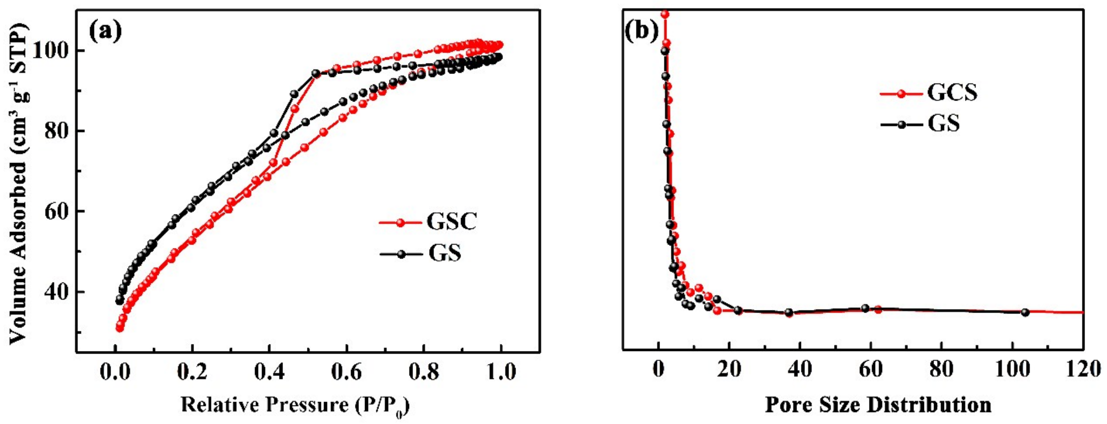

Fig. S6 (a) Nitrogen adsorption-desorption isotherms and (b) pore size distributions of GSC and GS.

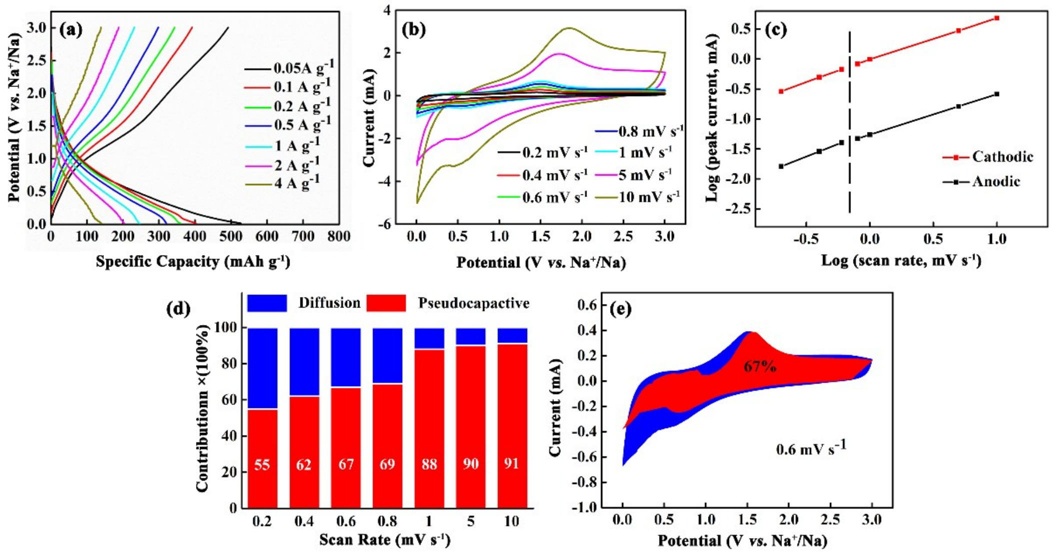

Fig. S7 (a) Cyclic voltammetry (CV) profiles of GS at various scan rates with the potential range between 0.01 and 3.0 V. (b) Determination of the *b* value using the relationship between peak current and scan rate. A *b* value of 0.5 or 1.0 represents diffusion-controlled or surface-controlled process, respectively. For the scan rates from 0.2 to 0.6 mV s^{-1}, the *b* values for the anodic and cathodic peaks are 0.84 and 0.77, respectively, revealing a primarily surface-controlled process. While increasing the scan rate to 0.6 mV s^{-1} and above, the slope is decreased and the *b* values decreased to 0.68 and 0.69 for the anodic and cathodic peaks, respectively, indicating a primarily diffusion-controlled process. (c) Normalized contribution ratio of pseudocapactive (red) and diffusion-controlled (blue) contribution at different scan rates. (d) Pseudocapactive (red) and diffusion-controlled (blue) contribution to charge storage of GS at 0.6 mV s^{-1}.

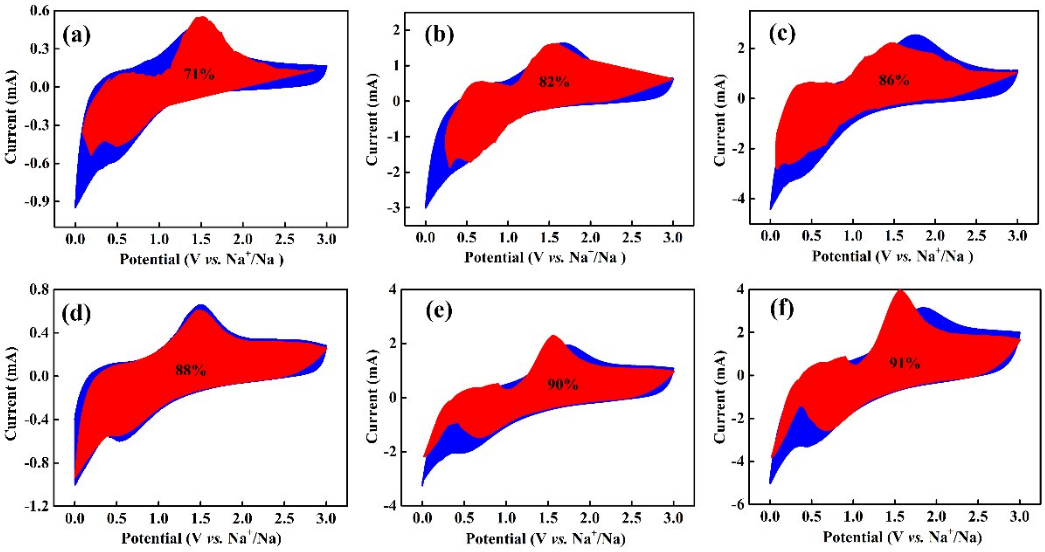

Fig. S8 Pseudocapacitive (red) and diffusion-controlled (blue) contribution to charge storage for GSC at (a) 1, (b) 5, (c) 10 mV s^{-1}, and for GS at (d) 1, (e) 5, (f) 10 mV s^{-1}.

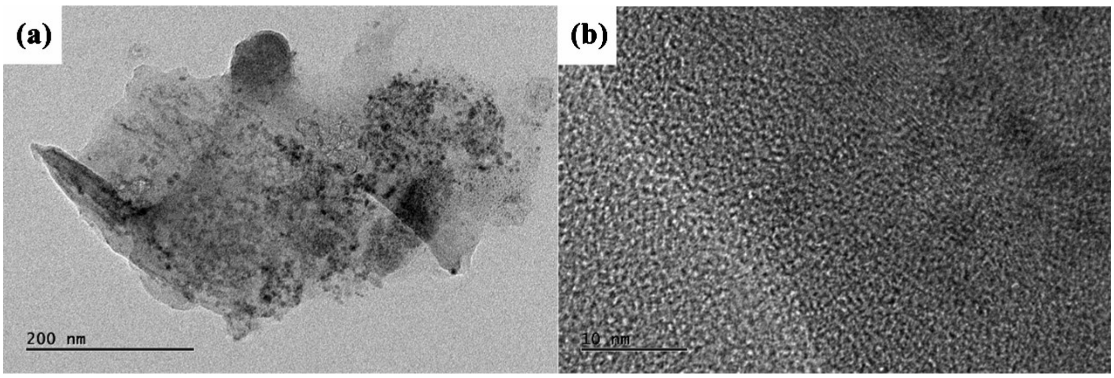

Fig. S9 Ex-situ TEM images of GSC after rate capability test (a) with low resolution and (b) with high resolution.

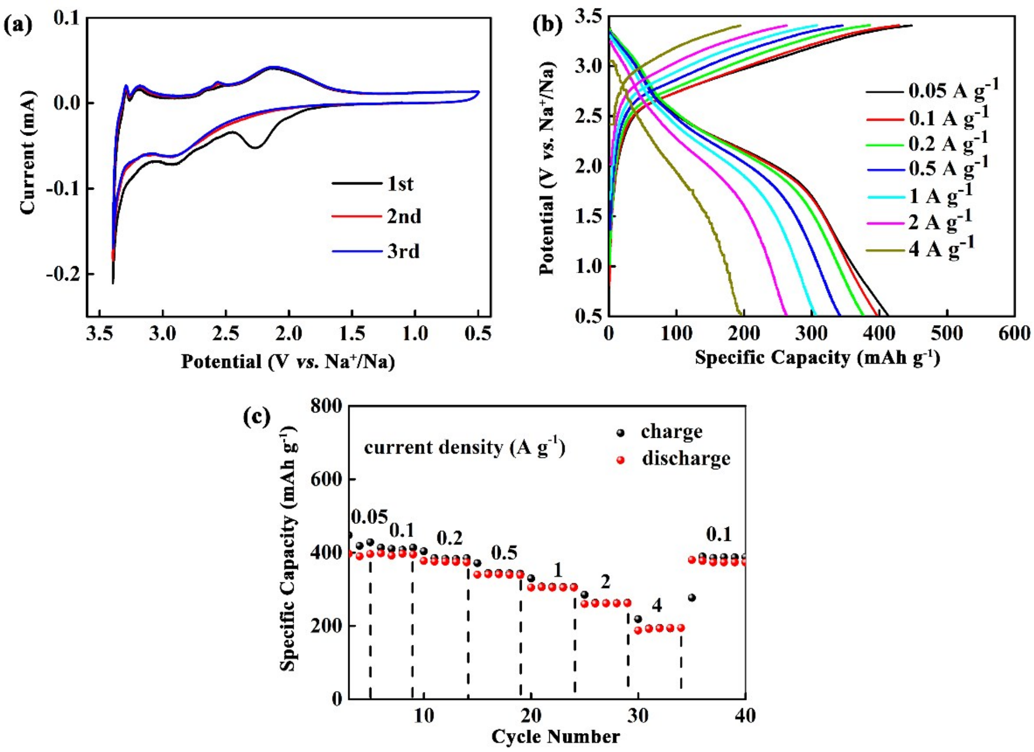

Fig. S10 (a) Cyclic voltammetry (CV) profiles of GSC-$Na_3V_2(PO_4)_3$ full cell at a scan rate of 0.1 mV s^{-1}. (b) Galvanostatic discharge-charge profiles of GSC-$Na_3V_2(PO_4)_3$ full cell within the potential window of 3.4-0.5 V at various current densities. (c) Rate performance of GSC-$Na_3V_2(PO_4)_3$ full cell at applied various current rates.

Table S1 The comparison of the electrochemical performance of the GSC electrode in this work with the state of the art results in previously reported researches on SnO_2-based systems

Sample	Cycling Capacity (mAh g^{-1})				Rate Capacity (mAh g^{-1})		
	3rd	30th	80th	Current Density			
This work	597	520	461	0.1 A g^{-1}	370 (0.5 A g^{-1})	270 (1 A g^{-1})	220 (2 A g^{-1})
SnO_2- graphene[1]	361	325		0.05 A g^{-1}	261 (0.2 A g^{-1})	213 (0.4 A g^{-1})	192 (0.8 A g^{-1})
SnO_2-graphene[2]	300	275	250	0.02 A g^{-1}	360 (0.2 A g^{-1})	290 (0.5 A g^{-1})	200 (1 A g^{-1})
SnO_2-C[3]	340	310	310	0.1 A g^{-1}	190 (0.4 A g^{-1})	144 (0.8 A g^{-1})	107 (1.6 A g^{-1})
SnO_2-C[4]	800	400	300	0.05 A g^{-1}	449 (0.2 A g^{-1})	284 (0.5 A g^{-1})	150 (1 A g^{-1})
SnO_2@PAIN[5]	240	180	190	0.3 A g^{-1}	150 (0.4 A g^{-1})	115 (0.8 A g^{-1})	110 (1 A g^{-1})
SnO_2-rGO[6]	360	410	400	0.05 A g^{-1}	307 (0.2 A g^{-1})	256 (0.8 A g^{-1})	200 (1.6 A g^{-1})
SnO_2-N/graphene[7]	325	305	280	0.02 A g^{-1}	220 (0.16 A g^{-1})	190 (0.32 A g^{-1})	170 (0.64 A g^{-1})
SnO_2-graphene[8]	580	350	320	0.02 A g^{-1}	299 (0.16 A g^{-1})	257 (0.32 A g^{-1})	220 (0.64 A g^{-1})
SnO_2-C[9]	380	300		0.05 A g^{-1}	300 (0.1 A g^{-1})	260 (0.2 A g^{-1})	192 (0.5 A g^{-1})
SnO_2 microfibers[10]	510	216		0.02 A g^{-1}	250 (0.16 A g^{-1})	150 (0.32 A g^{-1})	80 (0.64 A g^{-1})
PCNF@SnO_2@C[11]	430	378	370	0.05 A g^{-1}	190 (0.2 A g^{-1})	144 (0.4 A g^{-1})	107 (0.8 A g^{-1})
SnO_2-rGO[12]	435	440	390	0.1 A g^{-1}	250 (0.2 A g^{-1})	184 (0.5 A g^{-1})	121 (1 A g^{-1})
SnO_2-graphene[13]	353	302	287	0.1 A g^{-1}	275 (0.2 A g^{-1})	250 (0.4 A g^{-1})	221 (0.8 A g^{-1})
SnO2[14]	498	475	446	0.02 A g^{-1}	370 (0.04 A g^{-1})	250 (0.08 A g^{-1})	221 (0.16 A g^{-1})
SnO_2-graphene[15]	531	498	486	0.08 A g^{-1}	302 (0.16 A g^{-1})	278 (0.32 A g^{-1})	126 (0.64 A g^{-1})
C/SnO_2/CC[16]	500	430	360	0.1 C	422 (1 C)	391 (5 C)	342 (10 C)
Al_2O_3/SnO_2/CC[16]	450	405	400	0.1 C	331 (1 C)	239 (5 C)	89 (10 C)
SnO_2-C[17]	440	400	400	0.5C	298 (1 C)	202 (2 C)	121 (5 C)
SnO_2@MWCNT[18]	479	400		0.1 C	400 (0.2C)	280 (0.5C)	
SnO_2/carbon[19]	680	539		0.02 A g^{-1}	305 (0.18 A g^{-1})	150 (0.54 A g^{-1})	108 (1.2 A g^{-1})
SnO_2-N/graphene[20]	504	345		0.05 A g^{-1}	252 (0.2 A g^{-1})	238 (0.4 A g^{-1})	210 (0.8 A g^{-1})
SnO_2 nanowires [21]	220	201					
SnO_2/graphene[22]	348	320		0.05 A g^{-1}	262 (0.2 A g^{-1})	201 (0.4 A g^{-1})	150 (0.8 A g^{-1})
SnO_2-C[23]	380	295	290	0.1 A g^{-1}	332 (0.2 A g^{-1})	290 (0.5 A g^{-1})	215 (1 A g^{-1})
C@SnO_2@C[24]					368 (0.25 A g^{-1})	317 (0.5 A g^{-1})	263 (1 A g^{-1})

Table S2 Kinetic parameters of the GSC and GS electrodes after first reversible sodium storage.

Sample	R_{ct} (Ω)	$\boldsymbol{\sigma}$
GSC	60.13	27.96
GS	130.28	81.96

Table S3 Surface area and total pore volume of GSC and GS.

Sample	Surface area ($m^2\ g^{-1}$)	Total pore volume ($cm^3\ g^{-1}$)
GSC	189	0.15
GS	209	0.15

References

[1] L. Fan, X. Li, B. Yan, J. Feng, D. Xiong, D. Li, L. Gu, Y. Wen, S. Lawes, X. Sun, *Adv. Energy Mater.*, 2016, **6**, 1502057.

[2] J. Patr, H.-C. Chena, C.-H. Yang, C.-T. Hsieh, C.-Y. Su, J.-K. Chang, *Nano Energy*, 2016, **28**, 124-134.

[3] Z. Huang, H. Hou, G. Zou, J. Chen, Y. Zhang, H. Liao, S. Li, X. Ji, *Electrochim. Acta*, 2016, **214**, 156-164.

[4] Y. Cheng, J, Huang, J. Li, Z. Xu, L. Cao, H. Ouyang, J. Yan, H. Qi, *J. Alloy. Compd.*, 2016, **658**, 234-240.

[5] X. Zhao, Z. Zhang, F. Yang, Y. Fu, Y. Lai, J. Li, *RSC Adv.*, 2015, **5**, 31465-31471.

[6] Y. Zhang, J. Xie, S. Zhang, P. Zhu, G. Cao, X. Zhao, *Electrochim. Acta*, 2015, **151**, 8-15.

[7] X. Xie, D. Su, J. Zhang, S. Chen, A.K. Mondal, G. Wang, *Nanoscale*, 2015, **7**, 3164-3172.

[8] X. Xie, S. Chen, B. Sun, C. Wang, G. Wang, *ChemSusChem*, 2015, **8**, 2948-2955.

[9] Y.C. Lu, C. Ma, J. Alvarado, T. Kidera, N. Dimov, Y.S. Meng, S. Okada, *J. Power Sources*, 2015, **284**, 287-295.

[10] Y. Lu, M. Yanilmaz, C. Chen, M. Dirican, Y. Ge, J. Zhu, X. Zhang, *ChemElectroChem*, 2015, **2**, 1947-1956.

[11] Y. Liu, X. Fang, M. Ge, J. Rong, C. Shen, A. Zhang, H. A. Enaya, C. Zhou, *Nano Energy*, 2015, **16**, 399-407.

[12] Y.-X. Wang, Y.-G. Lim, M.-S. Park, S.-L. Chou, J.-H. Kim, H.-K. Liu, S.-X.

Dou, Y.-J. Kim, *J. Mater. Chem. A*, 2014, **2**, 529-534.

[13] S. Li, Y. Wang, J. Qiu, M. Ling, H. Wang, W. Martens, S. Zhang, *RSC Adv.*, 2014, **4**, 50148-50152.

[14] D. Su, C. Wang, H. Ahn, G. Wang, *Phys.Chem.Chem.Phys.*, 2013, **15**, 12543-12550.

[15] D. Su, H.-J. Ahn, G. Wang, *Chem. Commun.*, 2013, **49**, 3131-3133.

[16] M. Dirican, Y. Lu, Y. Ge, O. Yildiz, X. Zhang, *ACS Appl. Mater. Interfaces*, 2015, **7**, 18387−18396.

[17] R.S. Kalubarme, J.Y. Lee, C.J. Park, *ACS Appl. Mater. Interfaces*, 2015, **7**, 17226-17237.

[18] Y. Wang, D. Su, C. Wang, G. Wang, *Electrochem. Commun.*, 2013, **29**, 8-11.

[19] X. Lu, G. Wu, Q. Xiong, H. Qin, Z. Ji, H. Pan, *Electrochim. Acta*, 2017, **245**, 587–596.

[20] G.-Z. Wang, J.-M. Feng, L. Dong, X.-F. Li, D.-J. Li, *Applied Surface Science*, 2017, **396**, 269–277.

[21] S. Mukherjee, N. Schuppert, A. Bates, J. Jasinski, J.-E. Hong, M.J. Choi, S.Park, *J. Power Sources*, 2017, **347**, 201-209.

[22] Y. Wang, Y. Jin, C. Zhao, Y. Duan, X. He, M. Jia, *Mater. Lett.*, 2017, **191**, 169–172.

[23] X. Ao, J. Jiang, Y. Ruan, Z. Li, Y. Zhang, J. Sun, C. Wang, *J. Power Sources*, 2017, **359**, 340-348.

[24] J. Qin, N. Zhao, C. Shi, E. Liu, F. He, L. Ma, Q. Li, J. Li, C. He, *J. Mater. Chem.*

A, 2017, **5**, 10946–10956.